Phase-matching mechanism for high-photon-energy harmonics of a long trajectory driven by a midinfrared laser

Cheng Gong, Jiaming Jiang, Chuang Li, Liwei Song, Zhinan Zeng,* Jing Miao, Xiaochun Ge, Yinghui Zheng, Ruxin Li, and Zhizhan Xu

State Key Laboratory of High Field Laser Physics, Shanghai Institute of Optics and Fine Mechanics, Chinese Academy of Sciences, Shanghai 201800, China

(Received 27 September 2011; revised manuscript received 20 December 2011; published 8 March 2012)

High-order harmonics were generated with neon gas by using 12-fs midinfrared laser pulses with stabilized carrier-envelope phase (CEP). At some specific CEP, a broad "supercontinuum" of the extreme ultraviolet spectrum can be obtained. Two distinct continuous spectral regimes are found by numerical simulation, which come from two adjacent half cycles of the laser pulse. A phase-matching mechanism for high-photon-energy harmonics of a long trajectory driven by a midinfrared laser pulse is found.

DOI: 10.1103/PhysRevA.85.033410 PACS number(s): 32.80.Rm, 42.65.Ky, 32.80.Fb

I. INTRODUCTION

Since its discovery nearly two decades ago [1], high-order harmonic generation (HHG) appears to be the best candidate for generating a tabletop coherent extreme ultraviolet (XUV) light source. The harmonic emission process can be understood in the well-known three-step model [2,3]: First, the driving laser pulse ionizes the target atom, then the free electron is accelerated and driven back by the laser field to the parent ion where it finally can recombine and give rise to the emission of a high-energy photon. When long pulses are applied, the three-step process takes place every half cycle resulting in the creation of attosecond pulse trains [4]. However, a lot of applications, such as studying atoms or molecules on the electronic timescale [5–8], need an isolated attosecond pulse (IAP). In order to generate IAPs, various methods have been proposed, e.g., polarization gating [9], double optical gating [10], generalized double optical gating [11], a two-color driving pulse [12,13], and so on. The conceptually most straightforward method to generate isolated attosecond pulses is to produce the high harmonics with a very short linearly polarized pulse [14], which confines the emission process into a single optical cycle. However, the carrier-envelope phase (CEP) should be stabilized when a few-cycle driving laser is applied, because the CEP of the driving laser pulse will dramatically affect the emission spectra [15]. Furthermore, to get a short isolated attosecond pulse, the bandwidth of the continuous spectrum should be large enough. The cutoff law for HHG, $E_c = I_p + 3.17U_p$ [4,16] (I_p denotes the ionization potential of the target atom, $U_p = E_0^2/4\omega^2$ is the ponderomotive energy, E_0 is the peak electric field, and ω is the angular frequency of the driving laser), implies that pulses with longer wavelength can produce harmonics with shorter wavelengths, which offers the possibility to obtain a broad supercontinuum. On the other hand, the harmonics yield decreases very fast with increasing driving wavelength. The scaling of $\lambda^{-(5-6)}$ [17,18] was found. Therefore, favorable phase-matching conditions are very important for HHG driven by intense midinfrared laser pulses [19–21].

The rapid development in ultrafast laser technology has enabled the construction of high-power femtosecond optical parametric amplifiers (OPA), which can offer a CEP-stabilized few-cycle pulse at midinfrared wavelengths [22–27]. By using pulses with a wavelength between 1.5 and 2.0 μm, the maximum photon energies of high-order harmonics have been extended to ~160 eV [28] and ~220 eV [29], respectively. Recently, water-window HHG has been demonstrated by several groups [19–21,30,31]. High harmonics of ~420 eV have been obtained in a gas cell filled with Ne gas driven by 50-fs, 1500-nm driving laser pulses using a hollow fiber. Kapteyn *et al.* [20,21,30] have carefully investigated the phase-matching conditions for the water-window HHG driven by midinfrared laser pulses of different wavelengths. However, all of these works were done by using a midinfrared laser with randomly fluctuating CEP. In this paper, we investigate the CEP effect on XUV harmonic supercontinuum generation experimentally using a homemade few-cycle midinfrared femtosecond laser with stabilized CEP [26].

II. EXPERIMENT SCHEME AND RESULTS

The schematic of the experiment is shown in Fig. 1. The CEP-stabilized midinfrared femtosecond pulses used in our experiment are produced by a three-stage optical parametric amplifier (OPA) pumped by a commercial Ti:sapphire laser amplifier (Coherent LEGEND-HE-Cryo, 40 fs, 800 nm, 1 kHz, 10 mJ pulse energy). After passing through an argon-filled hollow fiber and the dispersion compensator (a pair of fused silica wedges), 0.7-mJ, 12-fs laser pulses at 1.75 μm central wavelength are obtained [25,26]. For high-harmonic generation, a steel tube with an inner diameter of 1 mm and filled with neon gas is used as a gas cell. The tube can be translated along the beam propagation direction by a high-precision translation stage. The CEP-stabilized few-cycle laser pulse is focused into the tube to generate the harmonics by a concave mirror with a focal length of 500 mm. After harmonics generation, the lower-order harmonics and the residual mid-IR driving laser are blocked by a 150-nm-thick aluminum foil. A spectrometer with a flat-field grating (Hitachi, 001-0266, 1200 lines/mm)

*zhinan_zeng@mail.siom.ac.cn

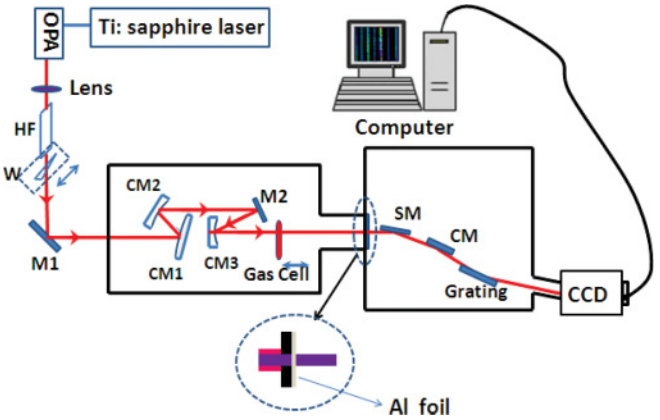

FIG. 1. (Color online) Schematic of experimental setup for generation of high-order harmonics with CEP-stabilized few-cycle midinfrared driving pulse. The CEP is stablized by the difference frequency generation (DFG) technique in the OPA system. The midinfrared laser pulse generated by the OPA is spectral broadened in the hollow fiber (HF) and compressed to be less than two cycles by the fused silica wedge (W). The few-cycle midinfrared laser pulse is focused by the mirror (CM3) into the gas cell to generate the harmonics. The Al foil is used to block the midinfrared laser pulse. The spherical mirror (SM) is used to image the exit of the gas cell on the entrance slit of the spectrometer on the horizontal axis.

and a soft-x-ray CCD (Andor, DO440) is used for measuring the HHG spectra. Before the spectrometer, a spherical concave gold mirror (SM) and a cylindrical concave gold mirror (CM) are used to collect the harmonics. The spherical mirror is used to image the harmonics of the exit of the gas on the entrance slit of the spectrometer. The cylindrical mirror is used to decrease the divergence angle of the harmonics to be detected by the CCD. The resolution of the spectrometer is ~0.07 nm at 72.5 eV. But, because of the limitation of the flat-field grating, the resolution of the spectrometer is only 0.05 nm at 150 eV, which is poor for the harmonics of high photon energy.

In the experiment, the energy of the laser pulse is fixed at ~0.68 mJ and the neon gas pressure is fixed at ~400 Torr. When the tube is located before the focal position of the concave mirror, the divergence angle of the high-order harmonics will be very large and the harmonics yield is low. When the tube is put 4 mm after the focal position, a bright XUV spectrum with a small divergence angle can be produced. Therefore, the position of the tube will be fixed for the following experiment while the CEP of the driving laser pulse is changed relatively from 0 to 2π in steps of $\pi/8$ radian by adjusting the thickness of the wedge. High-order harmonic spectra ranging from 68 to 160 eV at various CEPs (from 0 to π) are shown in Fig. 2. The Φ_0 is used in the figure because we do not know the absolute value of the CEPs in the experiment. In the figure, the modulation depths (modulation depth: $(I_{max} - I_{min})/(I_{max} + I_{min})$, where I_{max} and I_{min} are the maximum and minimum intensities of the harmonics, respectively) of the spectra near the aluminum absorption edge (about 72.5 eV) are very large at most of the CEPs. However, when the CEP is adjusted to $\Phi_0 + 5\pi/8$, the spectrum near the aluminum absorption edge becomes very smooth.

The spectra from 68 eV to the cutoff (~250 eV) are shown in Figs. 3(a) and 3(b) for a CEP of $\Phi_0 + \pi/8$ and $\Phi_0 + 5\pi/8$. The corresponding raw images obtained by the CCD are shown in Figs. 3(c) and 3(d), respectively. When the CEP is set to $\Phi_0 + 5\pi/8$, a very good continuum can be obtained near the absorption edge of the aluminum. When the CEP is changed by π to 2π, the result is similar to that of the CEP changed by 0 to

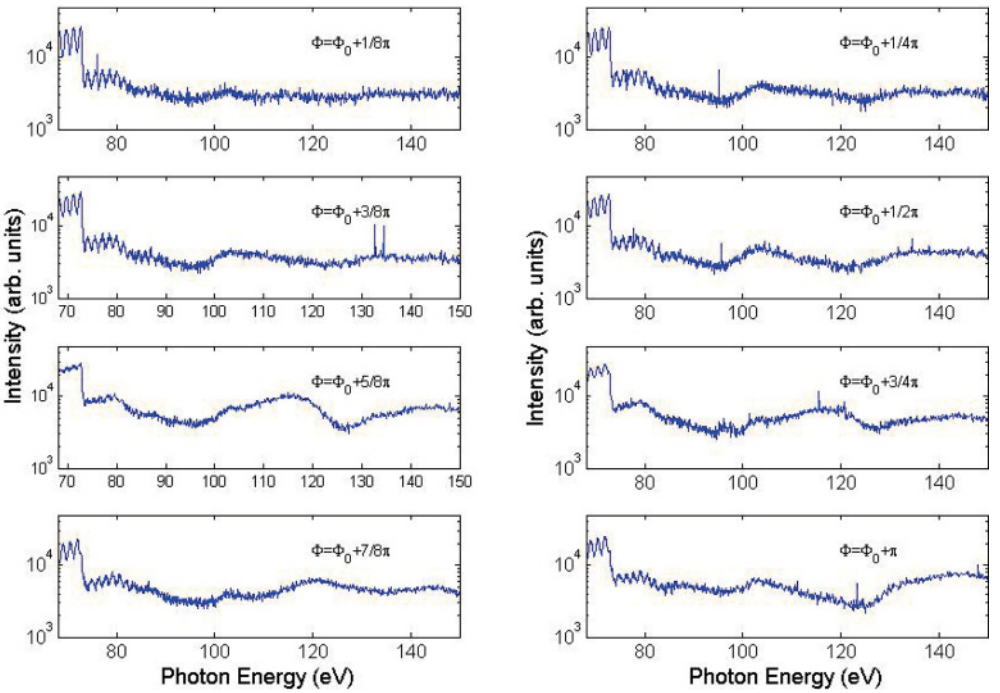

FIG. 2. (Color online) Spectra of XUV harmonics driven by 12-fs laser pulses with different CEPs. The Φ_0 is used in the figure because the absolute value of the CEP is unknown.

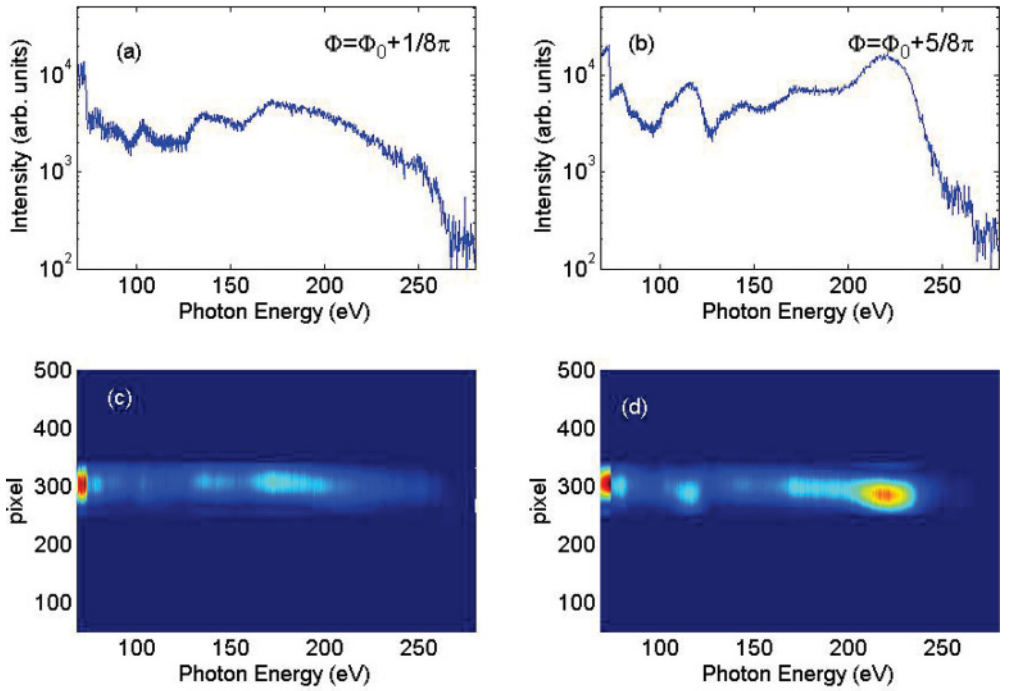

FIG. 3. (Color online) Harmonic spectra when CEP is changed by (a) $\pi/8$ and (b) $5\pi/8$. The corresponding original images obtained by CCD are shown in (c) and (d), respectively.

π (Fig. 1). A continuum can also be produced when the CEP is adjusted to $\Phi_0 + 13\pi/8$. Does this mean that a supercontinuum from about 70 eV to the cutoff is obtained? How can a two-cycle laser pulse generate such a broad continuum from 70 to 250 eV? The laser intensity in our experiment is about 3×10^{14} W/cm^2, which is much smaller than the saturation intensity of the neon gas. Therefore, the atoms will not be depleted in one half cycle to generate the supercontinuum [32]. To shed light on this, a numerical simulation considering the propagation effect has been performed. We use the first-order

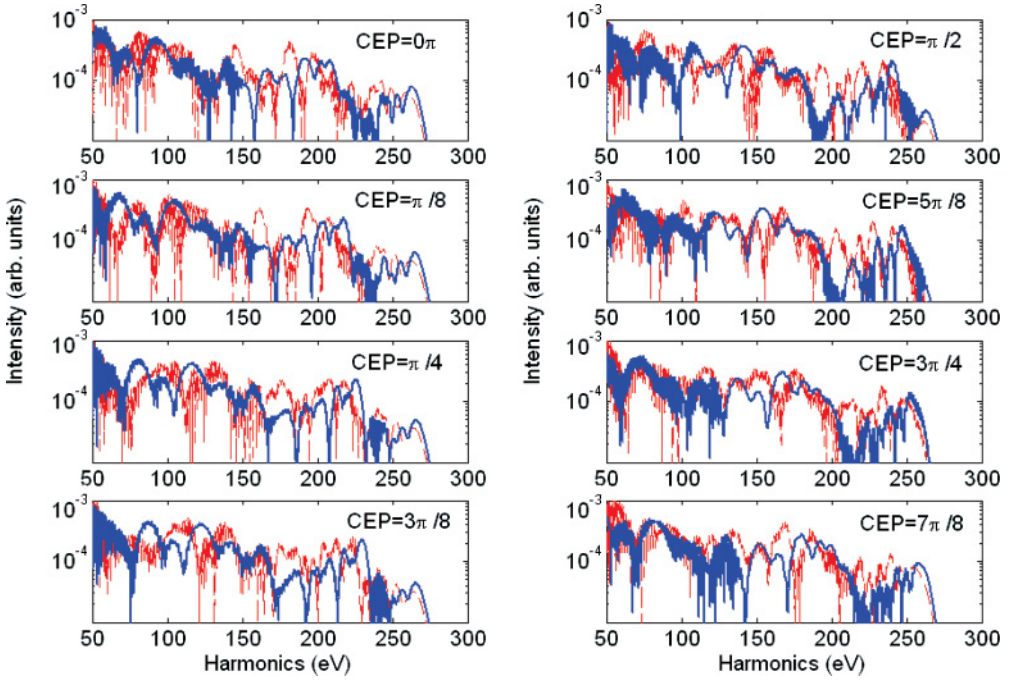

FIG. 4. (Color online) Numerical simulation of the HHG by the laser pulse of different CEPs. The blue solid lines show the on-axis harmonics of near field. The red dashed lines show on-axis harmonics of far field.

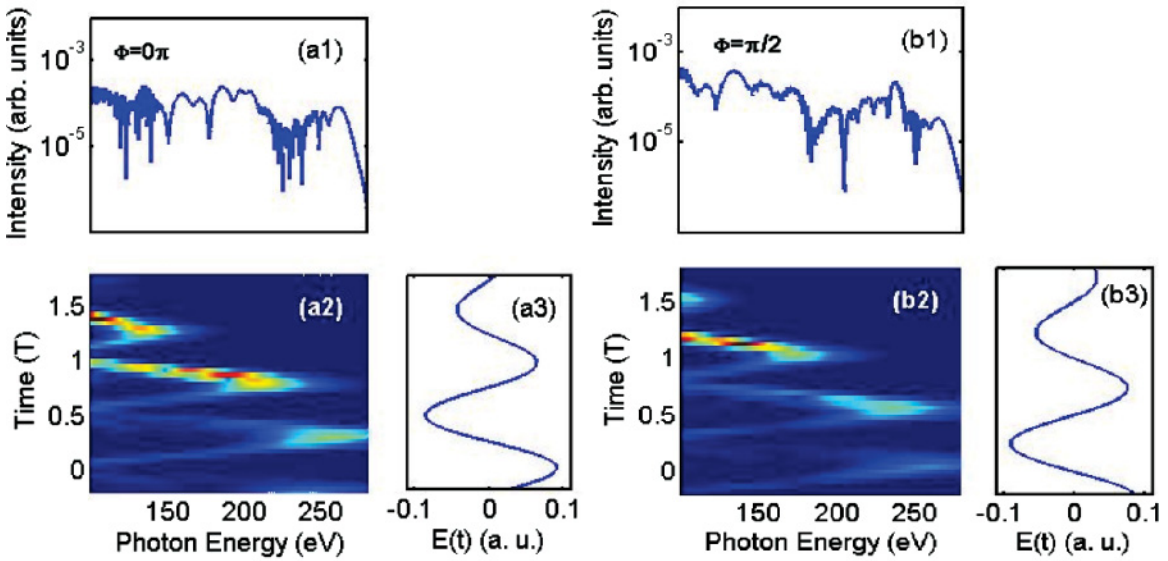

FIG. 5. (Color online) Harmonic spectra of different CEPs (a1), (b1); the corresponding result of the time-frequency analysis is shown in (a2) and (b2), respectively. Panels (a3) and (b3) show the corresponding electric field.

propagation (FOP) equation [33] to calculate the evolution of the laser field. The details of this method can be found in Ref. [34]. The time-dependent dipole moment of the atom is calculated by the Lewenstein model [4].

III. SIMULATION RESULTS

In the simulation, the original driving pulse is assumed to be Gaussian both in temporal and spatial domain with a central wavelength of 1800 nm, full width at half maximum (FWHM) pulse duration of 12 fs, a peak intensity of 3.0×10^{14} W/cm^2, and a waist of 160 μm. The temporal evolution of the laser's electric field is defined by $E(t) = E_0(t)\cos(\omega t + \Phi_0)$, where $E_0(t)$ is the Gaussian pulse envelope. This implies the assumption of a cosinelike field for $\Phi_0 = 0$. The gas pressure is fixed at 400 Torr. When the center of the gas medium is put 2.0 mm after the focal point, the simulation results reproduce our measurements well. The CEP is changed from 0 to $7\pi/8$ in steps of $\pi/8$. The corresponding on-axis harmonic spectrum is presented (Fig. 4, blue solid line). The continuum spectra are divided into two parts, the normal continuum in the cutoff regime [35], and a strange continuum in the plateau regime. The strange continuum ranges from 150 to 200 eV when Φ_0 is zero. For $\Phi_0 = \pi/2$, the strange continuum ranges from 100 to 150 eV. This means that the continuum moves when the CEP is changed. In our experiment, the resolution of the spectrometer is good enough for the low-photon-energy harmonics, e.g., ~0.07 nm at 72.5 eV. It is only 0.05 nm at 150 eV, which is not good enough to resolve harmonics at high photon energy. Therefore, the spectrum of the high photon energy always seems to be continuous. At lower photon energy, however, we can resolve harmonic structure if it is present. Indeed, we observe continuous spectra at low photon energies only for specific CEPs. The far-field harmonics are also shown in Fig. 4 (red dashed line). Some small modulations appear where the near-field harmonic spectrum is smooth.

The mechanism described in [35–37] can only explain the continuum in the cutoff region for the (rather long) pulse durations used in this work. What we observe, however, is a continuous spectrum that moves between the photon energies of 100 and 200 eV when the CEP is changed. A discrete spectrum can always be seen between these two parts. To find out the reason, a time-frequency analysis is done for the spectra in Fig. 4. The results for $\Phi_0 = 0$ and $\pi/2$ are presented in Figs. 5(a2) and 5(b2), which show that the photons in different parts of the spectra are generated in different half cycles of the laser pulse, hence the absence of the harmonic structure. The continuum in the cutoff regime is generated in the half cycle close to the peak of the laser pulse, while the continuum in the plateau regime is generated in the following half cycle on the trailing edge of the laser pulse. The long-trajectory harmonics of the latter are phase matched constructively, but the harmonics of the former are different, where only the high-photon-energy harmonics in the cutoff regime are constructively accumulated. Therefore, the emissions in this half cycle mainly contribute to the spectrum of the cutoff. These result in the two parts of the continuum in the spectrum.

IV. CLASSICAL ANALYSIS

Why are the long-trajectory harmonics dominant in the plateau regime? To understand this, we investigate the classical motion of the electron for each trajectory. For an electron ionized at t_i and recombining at t_r, the phase of the harmonics can be written as

$$\phi = \int_{t_i}^{t_f} \frac{1}{2} v(t)^2 dt + I_p(t_r - t_i) + E_h t_r, \qquad (1)$$

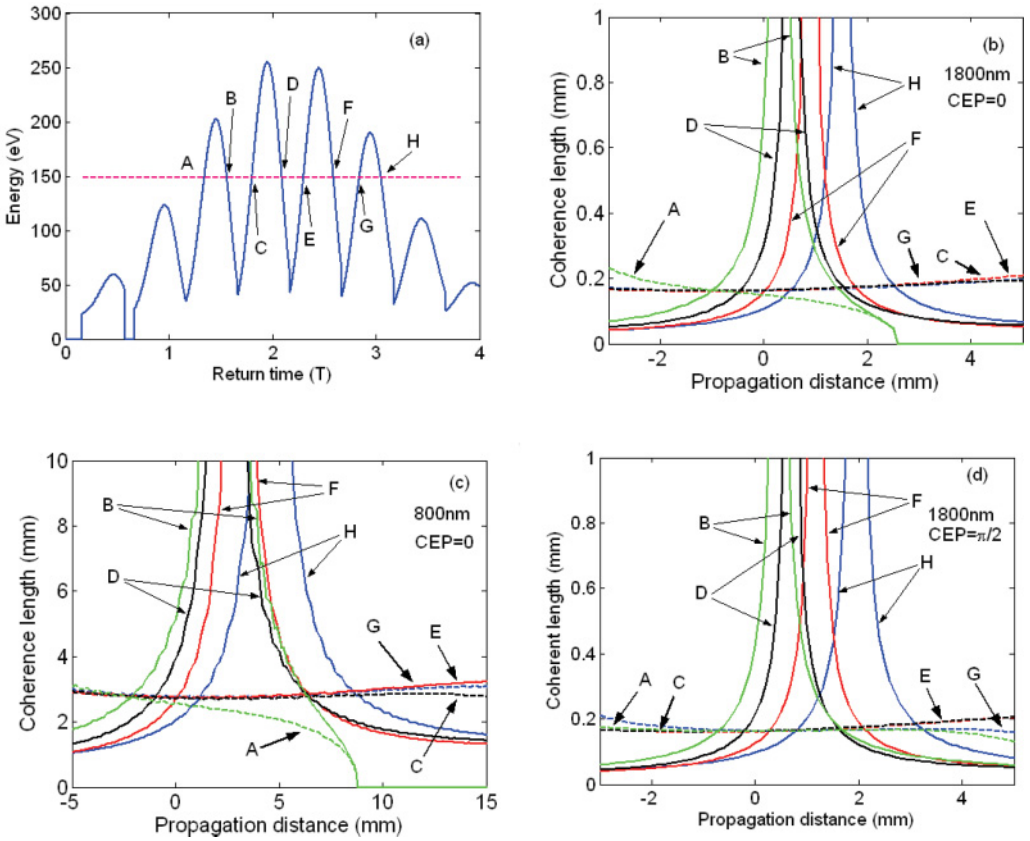

FIG. 6. (Color online) (a) Photon energy vs returning time; (b) coherence length of 150-eV harmonic of different trajectories generated by 1800-nm pulse along the propagation axis; (c) coherence length of 45-eV harmonic of different trajectories generated by 800-nm pulse. (d) Similar to (b), but the CEP is changed to be $\pi/2$.

where $v(t)$ is the velocity of the electron and I_p is the potential of the neon atom. E_h is the photon energy of the harmonic, which is $v(t_r)^2/2 + I_p$ here. The first two terms on the right-hand side denote the atomic intrinsic phase and the last term denotes the effect of the Gouy phase (when the Gouy phase is changed in the propagation, the return time t_r will change). With this phase, we can calculate the phase mismatch $\Delta k(z) = -\partial\phi/\partial z$ and the coherence length $L_{\rm coh} = \pi/|\Delta k(z)|$, where z is the propagation distance. Figure 6(b) shows the coherence lengths of the harmonics of different trajectory along the propagation axis, in which the wavelength of the driving pulse is 1800 nm and the CEP is zero. The photon energy of the harmonics is 150 eV, which is located in the middle of the plateau. The other conditions are the same as those in Fig. 5. Similar to previous work [38,39], the long-trajectory harmonics are well phase matched under a specific focal condition. Figure 6(c) shows the coherence length of a 45-eV harmonic generated by 800-nm pulses under the same conditions of Fig. 6(b). The coherence lengths of the short-trajectory harmonics can be about 3 mm in Fig. 6(c), but only 0.2 mm in Fig. 6(b). In general, the harmonic yield S_q can be written as [40]

$$S_q \propto L^2 \mathrm{sinc}^2\left(\frac{\Delta k\, L}{2\pi}\right) = L^2 \mathrm{sinc}^2\left(\frac{L}{2L_{\rm coh}}\right), \qquad (2)$$

where L is the length of the media and Δk is the wave vector mismatch. The function $\mathrm{sinc}(x)$ is defined by $\sin(\pi x)/(\pi x)$. In our experiment, the inner diameter of the steel tube is 1 mm. So, if an 800-nm laser pulse is used, the short-trajectory harmonics can build up along the propagation axis for $L \ll 2L_{\rm coh}$. On the other hand, if a 1800-nm laser pulse is used, the short-trajectory harmonics cannot be phase matched because the function $\mathrm{sinc}^2(x)$ will be very small for $x > 1$. Only the long-trajectory harmonics can be phase matched under the present specific focal conditions. Further, when few-cycle laser pulses are used, different long-trajectory harmonics can be phase matched at different positions [Figs. 6(b)–6(d)]. The maximum value of coherence length can be inferred for curve "H." The maximum is located at about $z = 1.5$ mm when 1800-nm laser pulses are used [Fig. 6(b)]. This explains why only the harmonics from the long-trajectory H can be phase matched in Fig. 5(a2). When the CEP is changed to be $\pi/2$ [Fig. 6(d)], we can draw a similar conclusion although the position of the maximum coherence length of curve H is changed slightly.

V. SUMMARY

In summary, we have investigated the HHG in Ne gas using a CEP-stabilized few-cycle 1.75-μm driving laser pulse. Our results show that at some specific CEP, a broad "supercontinuum" can be observed in the experiment. Further investigation by solving the propagation equation shows that

the continuous spectra are divided into two parts, which come from two adjacent half cycles of the laser pulse. The classical simulation for the electron of different trajectories shows that, when the midinfrared laser pulse is used, coherence lengths of the short-trajectory harmonics are all very small and only the long-trajectory harmonics can be accumulated constructively under some specific focal condition.

ACKNOWLEDGMENTS

This work is supported by the National Natural Science Foundation (Grants No. 10734080, No. 60921004, No. 10904157, No. 60978012, No. 61078022, and No. 60808008), 973Project (Grant No. 2011CB808103), and Shanghai Commission of Science and Technology (Grant No. 10QA1407600).This work was supported by Shanghai Supercomputer Center of China.

[1] P. Agostini and L. F. DiMauro, Rep. Prog. Phys. **67**, 813 (2004).

[2] P. B. Corkum, Phys. Rev. Lett. **71**, 1994 (1993).

[3] K. C. Kulander, K. J. Schafer, and J. L. Krause, in *Super-Intense Laser-Atom Physics*, NATO Advanced Study Institute, Series B: Physics, Vol. 316, edited by B. Piraux and K. Rzążewski (Plenum, New York, 1993), p. 95.

[4] M. Lewenstein, P. Balcou, M. Y. Ivanov, A. L'Huillier, and P. B. Corkum, Phys. Rev. A **49**, 2117 (1994).

[5] E. Goulielmakis, Z. Loh, A. Wirth, R. Santra, N. Rohringer, V. S. Yakovlev, S. Zherebtsov, T. Pfeifer, A. M. Azzeer, M. F. Kling, S. R. Leone, and F. Krausz, Nature **466**, 739 (2010).

[6] P. B. Corkum and F. Krausz, Nat. Phys. **3**, 381 (2007).

[7] H. Kapteyn, O. Cohen, I. P. Christov, and M. Murnane, Science **317**, 775 (2007).

[8] F. Krausz and M. Ivanov, Rev. Mod. Phys. **81**, 163 (2009).

[9] G. Sansone, E. Benedetti, F. Calegari, C. Vozzi, L. Avaldi, R. Flammini, L. Poletto, P. Villoresi, C. Altucci, R. Velotta, S. Stagira, S. D. Silvestri, and M. Nisoli, Science **314**, 443 (2008).

[10] H. Mashiko, S. Gilbertson, M. Chini, X. Feng, C. Yun, H. Wang, S. D. Khan, S. Chen, and Z. Chang, Opt. Lett. **34**, 3337 (2009).

[11] X. Feng, S. Gilbertson, H. Mashiko, H. Wang, S. D. Khan, M. Chini, Y. Wu, K. Zhao, and Z. Chang, Phys. Rev. Lett. **103**, 183901 (2009).

[12] N. Dudovich, O. Smirnova, J. Levesque, Y. Mairesse, M. Yu. Ivanov, D. M. Villeneuve, and P. B. Corkum, Nat. Phys. **2**, 781 (2006).

[13] Z. Zeng, Y. Cheng, X. Song, R. Li, and Z. Xu, Phys. Rev. Lett. **98**, 203901 (2007).

[14] E. Goulielmakis, M. Schultze, M. Hofstetter, V. S. Yakovlev, J. Gagnon, M. Uiberacker, A. L. Aquila, E. M. Gullikson, D. T. Attwood, R. Kienberger, F. Krausz, and U. Kleineberg, Science **320**, 1614 (2006).

[15] A. Baltuska, T. Udem, M. Uiberacker, M. Hentschel, E. Goullelmakis, C. Gohle, R. Hozlwarth, V. S. Yakovlev, A. Scrinzi, T. W. Hänsch, and F. Krause, Nature **421**, 611 (2003).

[16] K. C. Kulander, K. J. Schafer, and J. L. Krause, in *Atoms in Intense Radiation Fields*, edited by M. Gavrila (Academic Press, New York, 1992).

[17] J. Tate, T. Auguste, H. G. Muller, P. Salières, P. Agostini, and L. F. DiMauro, Phys. Rev. Lett. **98**, 013901 (2007).

[18] A. D. Shiner, C. Trallero-Herrero, N. Kajumba, H.-C. Bandulet, D. Comtois, F. Légaré, M. Giguère, J-C. Kieffer, P. B. Corkum, and D. M. Villeneuve, Phys. Rev. Lett. **103**, 093002 (2009).

[19] E. J. Takahashi, T. Kanai, K. L. Ishikawa, Y. Nabekawa, and K. Midorikawa, Phys. Rev. Lett. **101**, 253901 (2008).

[20] T. Popmintchev, M. C. Chen, O. Cohen, M. E. Grisham, J. J. Rocca, M. M. Murnane, and C. Kapteyn, Opt. Lett. **33**, 2128 (2008).

[21] T. Popmintchev, M. C. Chen, A. Bahabad, M. Gerrity, P. Sidorenko, O. Cohen, I. P. Christov, M. M. Murnane, and H. C. Kapteyn, Proc. Natl. Acad. Sci. USA **106**, 10516 (2009).

[22] A. Baltuska, M. Uiberacker, E. Goulielmakis, R. Kienberger, V. S. Yakovlev, T. Udem, T. W. Hänsch, and F. Krausz, IEEE J. Sel. Top. Quantum Electron. **9**, 972 (2003).

[23] X. Gu, G. Marcus, Y. Deng, T. Metzger, C. Teisset, N. Ishii, T. Fuji, A. Baltuska, R. Butkus, V. Pervak, H. Ishizuki, T. Taira, T. Kobayashi, R. Kienberger, and F. Krausz, Opt. Express **17**, 62 (2009).

[24] C. P. Hauri, R. B. Lopez-Martens, C. I. Blaga, K. D. Schultz, J. Cryan, R. Chirla, P. Colosimo, G. Doumy, A. M. March, C. Roedig, E. Sistrunk, J. Tate, J. Wheeler, L. F. DiMauro, and E. P. Power, Opt. Lett. **32**, 868 (2007).

[25] C. Zhang, P. Wei, Y. Huang, Y. Leng, Y. Zheng, Z. Zeng, R. Li, and Z. Xu, Opt. Lett. **34**, 2730 (2009).

[26] C. Li, D. Wang, L. Song, J. Liu, P. Liu, C. Xu, Y. Leng, R. Li, and Z. Xu, Opt. Express **19**, 6783 (2011).

[27] B. E. Schmidt, P. Béjot, M. Giguère, A. D. Shiner, C. Trallero-Herrero, É. Bisson, J. Kasparian, J.-P. Wolf, D. M. Villeneuve, J.-C. Kieffer, P. B. Corkum, and F. Légaré, Appl. Phys. Lett. **96**, 121109 (2010).

[28] B. Shan and Z. Chang, Phys. Rev. A **65**, 011804(R) (2001).

[29] P. Colosimo, G. Doumy, C. I. Blaga, J. Wheeler, J. Hauri, C. Hauri, F. Catoire, J. Tate, R. Chirla, A. M. March, G. G. Paulus, H. G. Muller, P. Agostini, and L. F. Dimauro, Nat. Phys. **4**, 386 (2008).

[30] M. C. Chen, P. Arpin, T. Popmintchev, M. Gerrity, B. Zhang, M. Seaberg, D. Popmintchev, M. M. Murnane, and H. C. Kapteyn, Phys. Rev. Lett. **105**, 173901 (2010).

[31] H. Xiong, H. Xu, Y. Fu, B. Zeng, W. Chu, Y. Cheng, Z. Xu, E. J. Takahashi, K. Midorikawa, X. Liu, and J. Chen, Opt. Lett. **34**, 1747 (2009).

[32] W. Cao, P. Lu, P. Lan, X. Wang, and G. Yang, Phys. Rev. A **74**, 063821 (2006).

[33] M. Geissler, G. Tempea, A. Scrinzi, M. Schnürer, F. Krausz, and T. Brabec, Phys. Rev. Lett. **83**, 2930 (1999).

[34] N. Milosevic, A. Scrinzi, and T. Brabec, Phys. Rev. Lett. **88**, 093905 (2002).

[35] A. de Bohan, P. Antoine, D. B. Milošević, and B. Piraux, Phys. Rev. Lett. **81**, 1837 (1998).

[36] G. Tempea, M. Geissler, and T. Brabec, J. Opt. Soc. Am. B **16**, 669 (1999).

[37] I. J. Sola, E. Mével, L. Elouga, E. Constant, V. Strelkov, L. Poletto, P. Villoresi, E. Benedetti, J.-P. Caumes, S. Stagira, C. Vozzi, G. Sansone, and M. Nisoli, Nat. Phys. **2**, 319 (2006).

[38] L. Chipperfield, P. Knight, J. Tisch, and J. Marangos, Opt. Commun. **264**, 494 (2006).

[39] M. B. Gaarde, J. L. Tate, and K. J. Schafer, J. Phys. B: At. Mol. Opt. Phys. **41**, 132001 (2008).

[40] C. M. Heyl, J. Gudde, U. Hofer, and A. L'Huillier, Phys. Rev. Lett. **107**, 033903 (2011).